PCCP

Cite this: *Phys. Chem. Chem. Phys.*, 2012, **14**, 4695–4702

www.rsc.org/pccp

PAPER

Structure-dependent optical properties of single-walled silicon nanotubes

Min Zhang,[a] ZhongMin Su*[a] and GuanHua Chen*[b]

Received 6th October 2011, Accepted 2nd February 2012
DOI: 10.1039/c2cp23164f

The electron excitations of Single-Walled Silicon Nanotubes (SWSiNTs), with sp^2 and sp^3 hybridization, were studied using the localized-density-matrix (LDM) method with INDO/S parameters. Strong anisotropic characteristics of the dynamic polarizabilities were found for all the nanotubes. The transitional intensity along the tubular axis is much larger than that perpendicular to the axis for all the nanotubes. The optical gaps of sp^3-hybridized infinitely-long pentagonal SWSiNTs are near 3.0 eV and 4.7 eV owing to σ–σ* transitions along the direction of the tubular axis. The optical gaps of sp^2-hybridized infinitely-long armchair SWSiNTs along the tube axis direction are about 0.7 eV and 2.4 eV for Si(3,3) SWSiNTs and 0.7 eV and 2.7 eV for Si(4,4) SWSiNTs. The former peak at 0.7 eV originated from π–π* electron transitions and the latter peak at 2.4 eV or 2.7 eV originated from σ–σ* electron transitions. Meanwhile, the intensities of π–π* electron transitions are stronger than those of σ–σ* electron transitions in SWSiNTs. The low sp^2 transition energy derived from the weak overlap of unpaired p_z orbitals of silicon atoms. Moreover, the electronic excitations of zigzag SWSiNTs are similar to those of armchair structures. This indicates that sp^2-hybridized silicon nanotubes possess much greater potential for application in optical fields.

Introduction

Since the discovery of carbon nanotubes (CNT) by Iijima[1] in 1991, intense experimental and theoretical studies on carbon nanotubes[2] and non-carbon nanotubes[3–6] have been investigated due to their fascinating properties and wide potential applications. Silicon is an element in the same column of the periodic table as carbon, and is a fundamental material in integrated circuits and the microelectronic semiconducting industry. Hence, attention has been focused on silicon nanotubes (SiNTs)[7] in chemical, physical, material and other fields.[8–14] Silicon tends to form four covalent bonds in a tetragonal coordination (sp^3 hybridization) and typically crystallizes in a diamond-like structure. Although stable Si═Si molecules[15–19] are possible, the π bond in silicon compounds is rather weak at about 25 kcal mol^{-1} (60 kcal mol^{-1} in carbon). On the contrary, carbon easily forms covalent bonds through sp, sp^2 or sp^3 hybridization.

One of the central questions is whether SiNTs based on sp^2 hybridization exist or not. SiNT structures based on sp^2 hybridization have been discussed theoretically.[3,8,11,20–36] Zhang *et al.*[24] proposed puckered surface SWSiNTs formed from PM3 simulations, although SWSiNTs were less stable than tetrahedral diamond-like structures. Our pervious study[28] suggested that SiNTs could be viewed as forming from a puckered layer, namely a strip cut from the crystal silicon along the {111} direction. The strip can be rolled up to make SiNTs along different directions, such as armchair nanotubes along the {100} direction and zigzag nanotubes along the {110} direction. The study also predicted the existence of stable silicon nanotubes, and that armchair nanotubes are the most reasonable structure due to the efficient overlap of p_z orbitals and the delocalization of π bonds. Zhang *et al.*[32] determined that the stability of SiNTs containing sp^2 hybridization increases in the order of smooth CNT-like tubes, gear-like tube, string-bean-like distortion (sp^2–sp^3) and so on. These studies indicate that SiNTs based on sp^2 hybridization are rational, although the stability is not strong due to weaker π bonds. Some proposed methods[3,8,22,37,38] to avoid threefold-coordinated dangling bonds in SiNTs are to saturate silicon atoms by electron transfer from encapsulated metals, and to bond the silicon by hydrogen and hydroxyl groups. It is well known that sp^3 hybridization of silicon in one-dimensional nanostructures favours the formation of nanowires rather than nanotubes. Zeng *et al.*[39] proposed a novel SiNT structure based on distorted tetrahedral bonds without encapsulated metals, although this kind of SiNT structure was previously suggested with encapsulated transition metals.[40–45]

There have been experimental reports that investigate sp^2- and sp^3-hybridized structures of SiNTs[9,46–58] simultaneously. One of the reported SiNTs is a defect single-crystal structure of bulk silicon with a diamond-like coordinated structure.[49] Other reported SiNTs, either polycrystalline or amorphous, are always combined with some amorphous silica.[31,46–48,51,59] Crescenzi *et al.* have synthesized unoxidized SiNTs in the diameter range

[a] *Institute of Functional Material Chemistry, Department of Chemistry, Northeast Normal University, Changchun 130024, P.R. China. E-mail: zmsu@nenu.edu.cn; Fax: +86-4318-5684009; Tel: +86-431-85269108*
[b] *Department of Chemistry, The University of Hong Kong, Pokfulam Road, Hong Kong SAR. E-mail: ghc@everest.hku.hk*

2 to 35 nm using the dc-arc plasma method.[52,56] The STM and TEM images proved the SiNTs' atomic arrangement were compatible with puckered structures and different chiralities, as in our proposed structures,[28] especially the armchair nanotube-like structures. *I–V* curves showed that SiNTs are semiconducting or metallic in character, which is in contrast to the non-metallic behaviour of silicon nanowires (SiNWs).[60] The study confirmed the presence of overlapping p_z orbitals in SiNTs, as found in CNTs, and the existence of sp^2 hybridization in SiNTs. The result of reflection electron energy loss experiments further verified the existence of π–π* electron transitions corresponding to sp^2-hybridized silicon in SiNTs.[56] Yamada *et al.*[57] also confirmed the presence of SiNTs composed of rolled-up quasi-two-dimensional honeycomb nets of silicon atoms with cylindrical symmetry and an inter-wall distance of 0.36 nm by HRTEM, as compared with the {111} inter-plane distance of 0.31 nm in silicon diamond structures.

Due to silicon's fundamental applications in electro-optical fields, investigations into SiNTs' optical properties are highly important. Experimentally Lee *et al.*[47] observed a peak centred at 2.06 eV in a photoluminescence (PL) spectra for SiNTs composed of amorphous Si about 50 nm in diameter and covered by an oxide layer of 10 nm on porous alumina. The peak position shifted to 2.21 eV after oxidization. Teo *et al.*[48] reported that a similar PL peak is close to 2.06 eV for normal SiNWs 20–50 nm in diameter, but the PL peak of uniform SiNWs 1–5 nm in diameter is about 1.72 eV and exhibits more intense (at least 10 times) luminescence than that of the former. Hu *et al.*[49] reported a weak emission peak near 2.76 eV in a room temperature cathode–luminescence spectrum from diamond-like cubic SiNTs with outer diameters of about 60–180 nm and wall thicknesses of about 20–60 nm that were grown on ZnS substrate. Xu *et al.*[53] reported that the turn-on field and threshold field for highly ordered SiNT arrays are about 5.1 V μm^{-1} and 7.3 V μm^{-1}, which are two of the lowest fields for Si field emission materials at technologically useful current densities. Patolsky[58] *et al.* reported a FET device based on sp^3-hybridized SiNTs, where the gate-voltage dependence is typical of p-type FETs and similar to that of nanowire-based FET devices. These studies illustrate the potential application of 1D silicon structures in the fields of nanooptoelectronic devices and field emitters. These discoveries also imply that the optical properties of SiNTs are directly related to their intrinsic structures. Hence, it is very significant to study the difference between the optical properties of sp^2 and sp^3 hybridized SiNTs and understand the origin of the difference.

In this paper, we report the optical properties of three different structures of SWSiNTs based on sp^2 and sp^3 hybridization with different tubular lengths using the LDM method and a INDO/S Hamiltonian. The SWSiNTs are the armchair, zigzag and polyhedral structures reported in *Chem. Phys. Lett.*[28] and *Proc. Natl. Acad. Sci. U. S. A.*[39] By comparison, the relation between optical properties and their intrinsic effect of sp^2 and sp^3 hybridization of the silicons in the nanotubes were obtained.

The INDO/S-LDM method

The linear polarization tensor α is defined as[61,62]

$$\alpha_{ij} = \left.\frac{dP_i(\omega)}{dP_j(\omega)}\right|_{E=0} \quad (1)$$

Where $P(\omega)$ is the electric polarization vector, $E(\omega)$ is the external electric field, and i and j are the indexes representing the x, y, and z components of a vector. The electric polarization is a physical observable and is defined by the expectation values of microscopic polarization operator $\hat{P}$

$$P(r,t) = Tr\,[\hat{P}(r)\,\rho(t)] \quad (2)$$

Where $\rho(t)$ is the reduced single-electron density matrix that can be obtained by solving the time-dependent Hartree–Fock (TDHF) equation of motion[63]

$$\left(i\hbar\frac{d}{dt} + \gamma\right)\rho(t) = [h, \rho(t)] \quad (3)$$

Where h is the Fock operator of the system and γ is the phenomenological dephasing constant. The INDO/S Hamiltonian[64–66] in the presence of an external field E is described as follows

$$\hat{H} = \sum_{ab}\sum_{i\in a,j\in b} t_{ij}c^{\dagger}_{ai}c_{bj} + \frac{1}{2}\sum_{a}\sum_{ijmn} V_a^{ij,mn}c^{\dagger}_{ai}c^{\dagger}_{am}c_{an}c_{aj} + \frac{1}{2}\sum_{a\neq b}\sum_{i\in a,j\in b}\gamma^{ij}_{ab}c^{\dagger}_{ai}c_{ai}c^{\dagger}_{bj}c_{bj} - E(t).\sum_{mn}\hat{P}^{mn}_{ab}c^{\dagger}_{am}c_{bn} \quad (4)$$

Where $c^{\dagger}_{ai}$ (c_{bj}) is the creation (annihilation) operator for an electron at a localized atomic spin-orbital $i(j)$ on atom $a(b)$. $V_a^{ij,mn}$ is the on-site repulsion, and γ^{ij}_{ab} stands for the two-center repulsion. The one-electron hopping integral t_{ij} may be expressed as

$$t_{ij} = \langle\chi^i_a|-\tfrac{1}{2}\nabla^2_r + U(r)|\chi^i_b\rangle \quad (5)$$

where $\chi_i(\chi_j)$ is the $i_{th}(j_{th})$ atomic orbital on atom $a(b)$, and $U(r)$ is the one-electron potential. The second and the third terms in eqn (4) represent the effective electron–electron Coulombic interaction. The last term describes the interaction between the valence electrons and an external electric field $E(t)$, and $\hat{P}$ is the molecular dipole moment operator. P^{ij}_{ab} is calculated by $\langle\chi^i_a|P|\chi^j_b\rangle$, neglecting the diatomic overlap. Taking into account the linear response only, the reduced single-electron density matrix $\rho(t)$ may be written as $\rho(t) = \rho(0) + \delta\rho$, where $\rho(0)$ is the ground-state reduced density matrix, and $\delta\rho$ is the field-induced density matrix deviation. Similarly, the Fock matrix h can be decomposed into $h = h(0) + \delta h$, where $h(0)$ is the Fock matrix in the absence of the external field:

$$h^{(0)mn}_{ab} = t^{mn}_{ab} + \delta_{ab}\left[2\sum_{ij\in a}\left(V_a^{mn,ij}\rho^{(0)ij}_{aa} - \frac{1}{2}V_a^{mi,nj}\rho^{(0)ij}_{aa}\right)\right] + \delta_{ab}\delta_{mn}\sum_{c\neq b}\sum_{l\in c}2\rho^{(0)ll}_{cc}\gamma^{ml}_{ac} - \rho^{(0)mn}_{ba}\gamma^{mn}_{ab} \quad (6)$$

Similarly, the field-induced Fock matrix can be written as

$$\delta h^{mn}_{ab} = \delta_{ab}\left[2\sum_{ij\in a}\left(V_a^{mn,ij}\delta\rho^{(0)ij}_{aa} - \frac{1}{2}V_a^{mi,nj}\delta\rho^{(0)ij}_{aa}\right)\right] + \delta_{ab}\delta_{mn}\sum_{c\neq b}\sum_{l\in c}2\delta\rho^{ll}_{cc}\gamma^{ml}_{ac} - \delta\rho^{mn}_{ba}\gamma^{mn}_{ab} \quad (7)$$

The single-electron density matrix follows the equation of motion:

$$(i\hbar\frac{d}{dt} + r)\delta\rho(t) = [h^{(0)}, \delta\rho(t)] + [\delta h(t), \rho^{(0)}] - E(t).[P, \rho^{(0)}] \quad (8)$$

where γ is the dephasing constant. More scientific details can be found from the references.[67–70]

The INDO/S method[64–66] is employed to generate the ground-state density matrices and Fock matrices from the reference of Zerner *et al.*,[71] and then the INDO/S-LDM method is employed to calculate absorption spectra. The dephasing parameter γ in the calculations of absorption spectra and LDM is 0.1 eV. No cut-off is adopted for ρ_0 (HF ground state reduced single-electron density matrix), induced density matrix and coulomb interaction. The anisotropy of electron excitations is investigated by calculating the dynamic polarizabilities for different directions. The excitation nature of main peaks is examined by the corresponding reduced single-electron density matrices. All the INDO/S calculations were carried out using our program LODESTAR V1.02.[67–69]

Results

A. Structures of silicon nanotubes

All of the structures[28,39] shown in Fig. 1 were optimized the B3LYP/6–31G(d) method using the Gaussian 03 program.[72] Both ends of all the systems are terminated with hydrogen atoms. Silicon's bond lengths, angles and dihedral angles were kept the same for identical situations in one nanotube, and then other SiNTs of different length were constructed with the optimized results with the repetitiveness of the 1D lattice. For the sp^3-hybridized SWSiNTs systems (a)–(c), the length of interlayer bonds (r_1 in Fig. 1 and Table 1) decreases with an increase in diameter. The corresponding interactions of interlayer bonds increase, which means that the interlayer interactions are important contributors in enhancing the stability of polyhedral nanotubes. It is also seen from the lengths of intralayer bonds (r_2 in Fig. 1 and Table 1) that the five-membered structure is just as stable as a planar ring structure. This was further verified from $\Delta E_{total}/n$ in Table 1.

All of the bond lengths in sp^2-hybridized SWSiNTs are shorter than those in sp^3-hybridized SWSiNTs. $\Delta E_{total}/n$ proves that the armchair SWSiNTs (systems (d) and (e)) are less stable than five-membered and six-membered polyhedral SWSiNTs. However, the stability of sp^2-hybridized SWSiNTs can be enhanced as the diameter increases due to an increase in electron delocalization and enhanced stability.[38] The length difference between intralayer (r_2) and interlayer (r_1) Si–Si bonds is also reduced as the diameter of sp^2-hybridized SWSiNT increases. However, the comparison of stabilities between the different types of SWSiNTS needs to be solved by further research and is not discussed here. The results in Table 1 are in good agreement with other studies.[25,27,31,32,36]

B. Validity for electron excitations of sp^2-conjugated systems

To validate the INDO/S parameters for the optical spectroscopy of sp^2-conjugated silicon systems, π–π* excitations of several planar Si_n *and* Si_nH_{n+2} (n = 12, 16, 20, 24) systems were first calculated with both methods: INDO/S-LDM and B3LYP-TDDFT/6–31G*. Si–Si and Si–H distances were 2.35 Å and 1.48 Å, and the Si–Si–Si angle was 2/3π. The difference between the two results is quite small (the main excitation energies are listed in Table 2), and the same descending trend

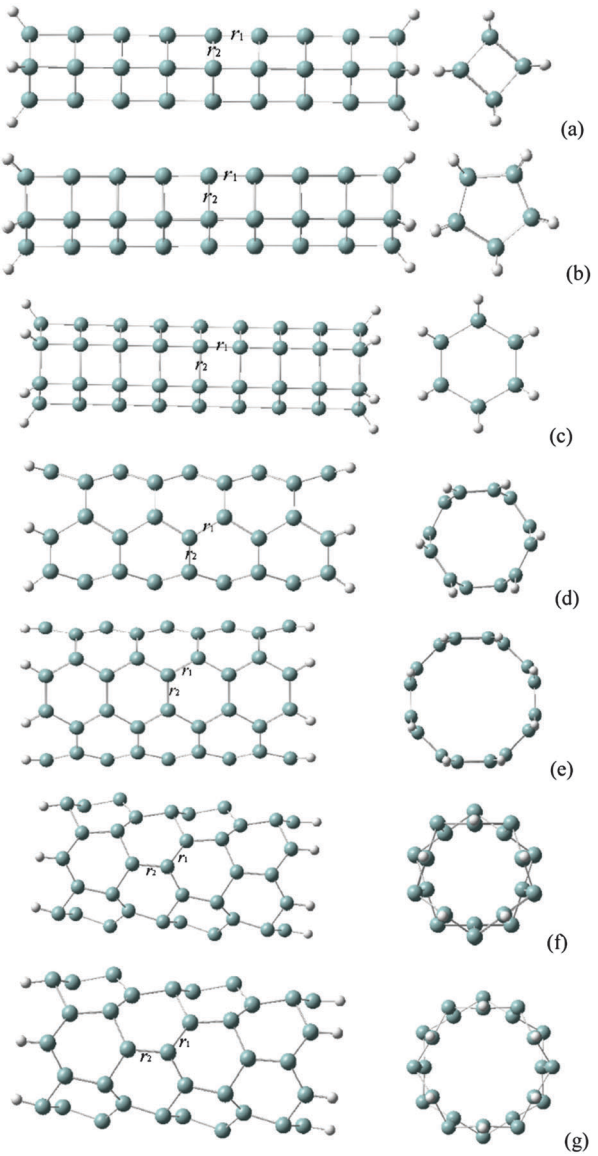

Fig. 1 Optimized structures of different SWSiNTs. The pentagonal SWSiNTs based on sp^3 hybridization: (a) square four-membered $Si_{36}H_8$[Si(4)], (b) pentagonal five-membered $Si_{45}H_{10}$[Si(5)] and (c) hexagonal six-membered $Si_{54}H_{12}$[Si(6)], and the armchair and zigzag SWSiNTs based on sp^2 hybridization: (d) armchair $Si_{54}H_{12}$[Si(3,3)], (e) armchair $Si_{72}H_{16}$[Si(4,4)], (f) zigzag $Si_{50}H_{10}$[Si(5,0)] and (g) zigzag $Si_{60}H_{12}$[Si(6,0)].

appears. The main transition is from π–π* excitations of Si═Si bonds. The results exhibit the feasibility of using INDO/S-LDM for sp^2-hybridized silicon systems. Hence, the original silicon INDO/S parameters by Zerner *et al.*[71] are adapted in the simulations of this article. The INDO/S-LDM method was also adapted to study the optical properties of hydrogenated silicon nanostructures.[73]

We calculated the electron excitations of a Si_{16} chain terminated with different atoms/groups, including one H atom, three H atoms, one hydroxyl and three hydroxyls. The main character of the electron excitations is almost the same as the pristine chain Si_{16} and the transition peaks remain nearly constant. For example, the strongest excitation of n–Si_{16} near

Table 1 Main results of the optimized SWSiNTs in Fig. 1

	Bond length/Å		Diameter/Å	$\Delta E_{HUMO-HOMO}$/eV	$\Delta E_{total}/n$/eV
	r_1	r_2			
(a) Si(4)	2.418	2.437	3.446	0.339	0.000[c]
(b) Si(5)	2.423	2.422	4.121	0.852	−1.551
(c) Si(6)	2.420	2.418	4.836	0.897	−1.506
(d) Si(3,3)	2.275	2.245	6.616	0.850	−0.609
(e) Si(4,4)	2.258	2.260	8.772	0.413	−1.329
(f) Si(5,0)	2.304	2.323	5.836(1.311)[a]	0.300	0.000[c]
(g) Si(6,0)	2.297	2.313	6.896(1.192)[a]	0.252	−0.246

[a] Internal diameter for puckered zigzag SiNTs, and the difference between internal and external diameters shown in parentheses. [b] n denotes the number of silicon atoms in one layer. [c] Polyhedral and armchair SiNTs referred to system a, and zigzag SiNTs referred to system g due to different atom numbers in SiNTs.

Table 2 The excitation energies of single chains, Si_n *and* Si_nH_{n+2}

	B3LYP-TDDFT/6–31G*	INDO/S
Si_{12}	1.55(strong)	1.54(strong)
	3.32(weak)	3.02(weak)
Si_{16}	1.29(strong)	1.33(strong)
	2.89(weak)	2.68(weak)
Si_{20}	1.14(strong)	1.06(strong)
	2.51(weak)	2.34(weak)
Si_{24}	1.00(strong)	0.90(strong)
	2.25(weak)	2.09(weak)
$Si_{12}H_{14}$	1.32(strong)	1.56(strong)
	2.95(weak)	2.66(weak)
$Si_{16}H_{18}$	1.10(strong)	1.32(strong)
	2.26(weak)	2.55(weak)
$Si_{20}H_{22}$	0.95(strong)	1.16(strong)
	1.99(weak)	2.28(weak)
$Si_{24}H_{26}$	0.84(strong)	1.04(strong)
	1.80(weak)	2.07(weak)

1.0 eV blue-shifts only 0.06 eV, because the optical properties of silicon clusters originate predominantly from electron excitations of the silicon skeletons. The overlap between silicon's orbitals (both π and σ bonds) is not strong, so the corresponding excitations occur first. Hence, the optical properties of hydrogen-terminated SWSiNTs are feasible. The experimental results of Uchiyama *et al.* agree with our conclusion that the longest-wavelength absorption maximum of UV–Vis spectra of R′–Si═Si–Si═Si–R′ ranges from 2.33 eV to 2.43 eV for different substituents, including aromatic radicals.[74]

C. Electron excitations of sp^3-hybridized SWSiNTs

As discussed in section A, the basic stability information on SWSiNTs has been obtained. The most stable polyhedral five-membered SWSiNTs were selected to further explore electron excitations of sp^3-hybridized SWSiNTs. Fig. 2 presents the calculated electron excitations (from $Si_{25}H_{10}$ ~1 nm to $Si_{125}H_{10}$ ~6 nm in length) using INDO/S-LDM. The length of $Si_{125}H_{10}$ is longer than the limit of silicon's free-exciton Bohr length (4.3 nm).[75]

The results show that the low-energy electron excitations (below 5.0 eV) are very weak in the vertical SWSiNT direction (Fig. 2a), and the intensity is still weak for the longest SWSiNT. The lowest-peak around 1.5 eV seems to be constant and the intensity increases with increases in the SWSiNTs' length. The electron excitations parallel to the SWSiNT direction (Fig. 2b) look completely different. The excitation intensities are much stronger than those in the perpendicular direction, and the intensities of a characteristic peak (arrow shown in Fig. 2b) increased dramatically. The peaks red-shift from 4.048 eV in $Si_{65}H_{10}$ to 3.557eV in $Si_{125}H_{10}$. The shoulder peak around 2.9 eV shows a similar trend to the peak around 1.5 eV in the vertical SWSiNT direction.

In order to identify the nature of the transition in the tubular direction, the ground density matrix and four important excited induced density matrixes ($\Delta\rho$) of $Si_{125}H_{10}$ were examined using INDO/S-LDM. The results are shown in Fig. 3a–e. Atomic orbital representation is employed. The atomic indices were assigned increasing from one end of the tube to another, and the orbital indices were arranged in the order of 2s, $2p_x$, $2p_y$, and $2p_z$. The absolute values of $\Delta\rho$ elements are shown in the contour plots. From the contour plots in Fig. 3a, it can be observed that the whole nanotube is constituted of σ bonds. The excited-states have a longer interactive distance of induced density matrix and coulomb interaction than the ground-state, although all four peaks mainly originate from σ–σ* transitions. The shoulder peak at 2.914 eV in Fig. 3b is attributed to a σ–σ* excitation of short distance and partly localized at two ends of the nanotube. Hence, it exists in all the SWSiNTs around the same energy. We speculate that the peak originates from a σ bond between adjacent distorted sp^3-hybridized silicon and partly from the π_σ–π_σ orbital interaction between the parallel rings, as illustrated recently by Hoffmann *et al.*[76] in similar carbon systems. Hence, the corresponding transition energy is lower than those of normal silicon σ–σ* transitions.[77,78] This peak can't be observed in multi-walled SiNTs based on fourfold-coordinated silicons, because there are no π_σ–π_σ bonds. The peaks at 3.557 eV and 5.010 eV (Fig. 3c and d) are mainly attributed to the excitation of the nanotube body. Although the peak at 5.262 eV (Fig. 3e) is attributed to more the ends and less to the body than the

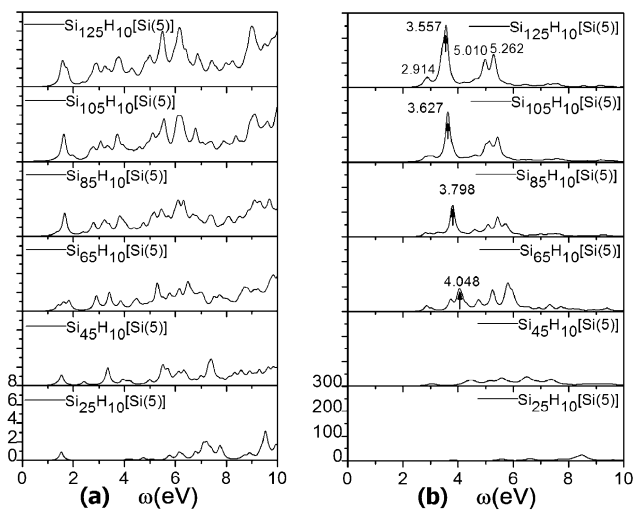

Fig. 2 Electron excitations of sp^3-hybridized five-membered polyhedral SWSiNTs [Si(5)]: (a) external field E is perpendicular to the tubular axis ($E\perp$ tube) and (b) external field E is parallel with the tubular axis ($E\|$ tube). The arrow indicates the uppermost absorption peak for each nanotube.

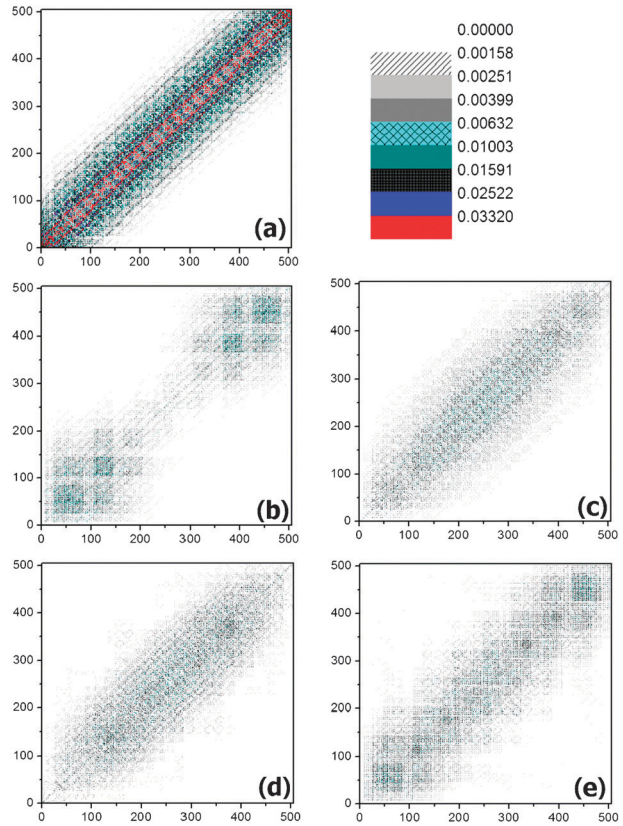

Fig. 3 The ground and induced density matrix ($\Delta\rho$) of five-membered polyhedral SWSiNT $Si_{125}H_{10}$[Si(5)] in the parallel tubular axis direction: (a) ground state, (b) 2.914 eV, (c) 3.557 eV, (d) 5.010 eV and (e) 5.262 eV (dephasing constant is 0.1 eV in the calculation).

peak at 5.010 eV, they possess a similar transition character. Hence, the last two peaks at 5.010 eV and 5.262 eV will merge into one as the SWSiNT length increases. Consequently, the peaks at 3.537 eV and 5.010 eV are the diagnostic electron excitation of five-membered polyhedral SWSiNTs. A peak around 3.5 eV can also be found from SiNWs, which originates from the quantum size effect,[79] and varies with the size and crystalline direction of the silicon systems.

The relationships between the last three excitation energy gaps of five-membered polyhedral SWSiNT and $1/N$ are plotted in Fig. 4 after linear fitting, where N is the number of silicon atoms. The excitation energies of infinitely long nanotubes are 2.998 eV, 4.652 eV and 4.754 eV. An interesting find is that the first peak of 2.998 eV is near the shoulder peak of π_σ–π_σ transition and the last two peaks are very close each other. Hence, based on our study, only two peaks would be experimentally observed at ~3.0 and 4.7 eV. The peaks of ~3.0 and 4.7 eV are characteristic absorption peaks of electron excitations of sp^3-hybridized SiNTs according to INDO/S-LDM. The peak at 4.7 eV is extremely close to the cohesion energy of silicon, 4.63 eV, which further proves the validity of our simulation. The excitation at ~3.0 eV corresponding with silicon's sp^3 hybridization is also consistent with results in other silicon nanostructures.[73]

The SWSiNT $Si_{65}H_{10}$ exhibits the essence of five-membered polyhedral electron excitations. The excitations of four-membered polyhedral $Si_{52}H_8$ and six-membered polyhedral $Si_{78}H_{12}$ were calculated and compared (shown in Fig. 5), since their tubular lengths are the same as five-membered polyhedral $Si_{65}H_{10}$. Their electron excitations are similar in the $E\perp$ tube direction, and no strong peak can be observed. The diagnostic transition in the $E||$ tube direction blue-shifts with an increase in the SWSiNTs diameter (shown with arrows in Fig. 5b).

D. Electron excitations of sp^2-hybridized SWSiNTs

The electron excitations of two types of sp^2-hybridized SWSiNTs, armchair and zigzag nanotubes, were calculated and compared with each other. Armchair and zigzag SWSiNTs have approximately equivalent conjugated six-membered circles along the tubular direction. They are: armchair $Si_{78}H_{12}$[Si(3,3)] and $Si_{112}H_{16}$[Si(4,4)], and zigzag $Si_{70}H_{10}$[Si(5,0)] and $Si_{84}H_{12}$[Si(6,0)]. Polyhedral $Si_{78}H_{12}$[Si(6)] was compared with armchair SWSiNT $Si_{78}H_{12}$[Si(3,3)], because they possess the same number of atoms. On the other hand, the lengths of [Si(6)] and [Si(3,3)] nanotubes are quite different. The calculated spectra of the five nanotubes in both directions are shown in Fig. 6. It can be observed from Fig. 5 and 6 that the excitation intensities of sp^2-hybridized SWSiNTs are higher than those based on sp^3 hybridization in both directions for the peaks below 4.0 eV. Armchair $Si_{78}H_{12}$[Si(3,3)] and $Si_{112}H_{16}$[Si(4,4)] both display a stronger excitation of σ–σ* transitions about 3.0 eV than polyhedral $Si_{78}H_{12}$[Si(6)] in addition to the lower excitation energy. A distinct excitation peak below 1.4 eV is observed, and the corresponding energy is much lower than the σ–σ* bond energy. From our previous study,[28] we know that the overlap of silicon p_z orbitals forms delocalized π bonds in armchair SWSiNTs. Hence, the electron excitations below 2.0 eV are probably π–π* transitions. Meanwhile, π–π* transitions usually display a higher intensity than σ–σ* transitions. Another feature is that the first diagnostic transition red-shifts and the second diagnostic transition blue-shifts for sp^2-hybridized SWSiNTs as the diameter increases (Fig. 6b).

The bond lengths in zigzag SWSiNTs are a little longer than those in armchair SWSiNTs, but the intensities of the excitations below 4.0 eV are stronger in zigzag SWSiNTs than in polyhedral SWSiNTs. The differences of the Si–Si bond lengths between armchair [Si(3,3)] and zigzag[Si(6,0)] are 0.02 Å for $_{r1}$ and 0.07 Å for r_2, but their peaks display a similar transitional character. The peaks of zigzag [Si(5,0)] are similar with others, although there is a node perpendicular to the axis that is very unfavourable to electron delocalization.[28] The peak at 0.918 eV from the π–π*

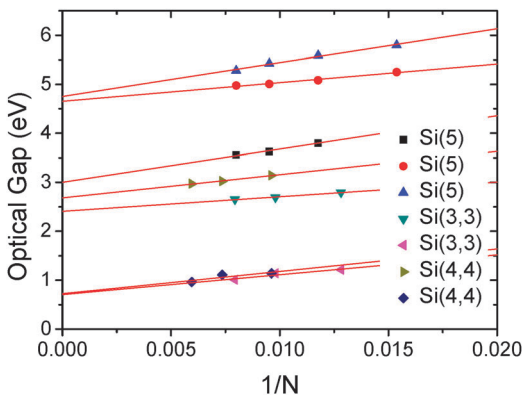

Fig. 4 Optical gap *via* $1/N$ for SWSiNTs.

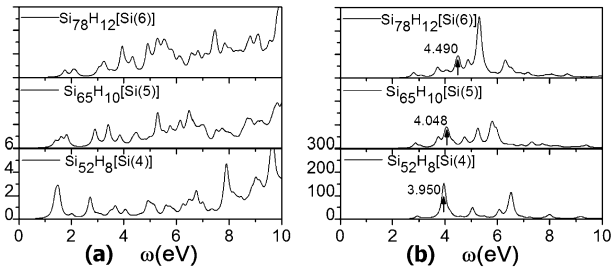

Fig. 5 Electron excitations of polyhedral SWSiNTs $Si_{52}H_8$[Si(4)], $Si_{65}H_{10}$[Si(5)] and $Si_{78}H_{12}$[Si(6)]: (a) along the $E\perp$ tube direction and (b) along the $E||$ tube direction.

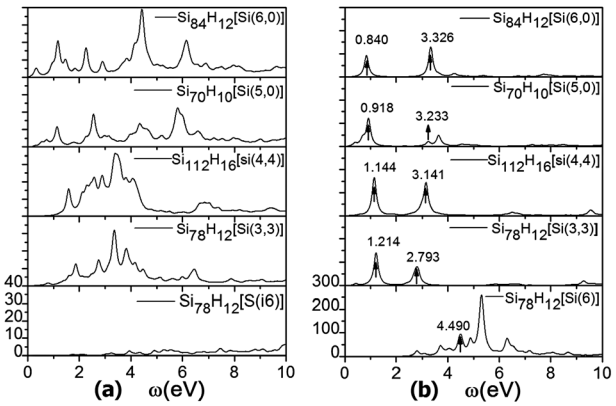

Fig. 6 Electron excitations of different nanotubes with the same length: (a) along the $E\perp$ tube direction and (b) along the $E||$ tube direction.

transition in [Si(5,0)] SWSiNTs is only a little weaker than the peak in [Si(6,0)] SWSiNTs. It reflects that the weak overlap between p_z orbitals contributes to the spectra and electron excitation in spite of its small effect on stability. The similar transition peaks in four sp^2-hybridized SWSiNTs indicates that the tubular chirality has limited impact on electron excitations, which is the same trend as found for carbon nanotubes.[67] Moreover, the excitation energy in armchair SWSiNTs along the {100} direction is less than that in zigzag SWSiNTs along the silicon {110} direction, which was also found for SiNWs.[79]

Fig. 7 and 8 shows the calculated excitation spectra of three armchair [Si(3,3)] nanotubes, $Si_{78}H_{12}$, $Si_{85}H_{12}$, $Si_{105}H_{12}$ and three armchair [Si(4,4)] nanotubes, $Si_{102}H_{16}$, $Si_{136}H_{16}$, $Si_{168}H_{16}$. The π–π* transitional energy of [Si(4,4)] along the tubular direction is a little higher than that of [Si(3,3)]. The peaks of the main excitations in the perpendicular tubular direction have blue-shifted slightly as the length increases (Fig. 7a and 8a), while the intensities are unchanged. However, in the parallel tubular direction the excitation intensities increase and the two main peaks both red-shift (Fig. 7b and 8b). This trend is the same as found for carbon nanotubes.[80] The peaks of polyhedral SiNT above 4.5 eV disappear.

Furthermore, in order to understand the nature of the transition in the parallel direction, the ground and two important excited induced density matrixes ($\Delta\rho$) of $Si_{126}H_{12}$[Si(3,3)] were calculated using INDO/S-LDM. The results are shown in Fig. 9 with the same reference contours. The atomic orbital indices are arranged as in Fig. 3. The absolute values of the $\Delta\rho$ elements and are also used as in Fig. 3. From the contour plots for ground state in Fig. 9a, it is observed that the armchair nanotube consists of σ bonds and delocalized π bonds. The first peak at 1.0 eV displays approximately the same interaction distance in an induced density matrix and coulomb interaction as the ground-state. It certifies that the corresponding excitation is a π–π* transition. The peak at 2.65 eV displays a shorter distance in an induced density matrix and coulomb interaction than the former peak. It is similar to interaction distance shown in Fig. 3c, although its value of $\Delta\rho$ elements is lower. It proves that the corresponding excitation is σ–σ* transition.

The relationships between the major-peak energies in armchair [Si(3,3)] and [Si(4,4)] and $1/N$ are also plotted in Fig. 4. The optical gaps of the infinitely long [Si(3,3)] SWSiNT along the tubular axis direction are about 0.7 eV and 2.4 eV, and those of the infinitely long [Si(4,4)] are 0.7 eV and 2.7 eV.

From these calculations on sp^2-hybridized SWSiNTs, we can conclude that one π–π* peak of electron excitations along the different tube directions is below 1.0 eV. The σ–σ* electron excitation around 2.7 eV is the only strong peak without other significant excitations. These results reflect that sp^2-conjugated SiNTs possess more applicable optical potential than sp^3-hybridized SiNTs.

E. Perspective on experimental results

Unfortunately, we can't compare our results with the experimental data directly. Firstly, there is currently no report on the SWSiNT spectrum. Secondly, it is known from our simulations and experimental data that the optical property changes dramatically with the diameter of SiNTs.[48] Thirdly, the oxidization layer[47] and other impurities also affect the spectrum peak.

However, we still can get some clue from our calculations on the sp^3- and sp^2- hybridized SWSiNTs, because they all display different characteristics of electron excitations. The σ–σ* transition energy for sp^3-hybridized SiNTs is higher than that for sp^2-hybridized SiNTs. For sp^3-hybridized SWSiNTs, the peaks located at ~ 3.0 eV and 4.5 eV are both due to σ–σ* electron transitions. For sp^2-hybridized SWSiNTs, one peak below 2.7 eV is mainly owing to σ–σ* electron transitions and the other below 1.0 eV is owing to π–π* electron transitions.

Experimentally, two peaks near 2.06 eV (600 nm) and 2.76 eV (450 nm) are observed in luminescence (PL) spectra for SiNTs and SiNWs prepared by different groups,[47–49] respectively.

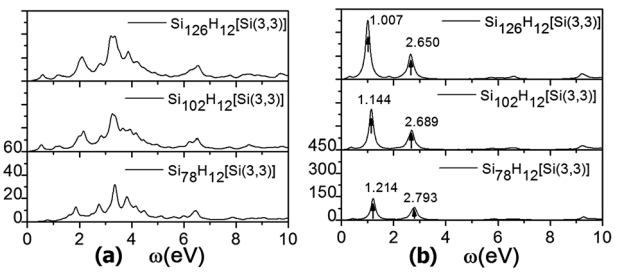

Fig. 7 Electron excitations of armchair [Si(3,3)] $Si_{78}H_{12}$, $Si_{85}H_{12}$, $Si_{105}H_{12}$: (a) along the $E\perp$ tube direction and (b) along the $E||$ tube direction.

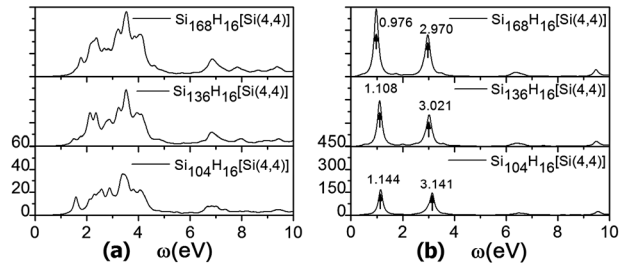

Fig. 8 Electron excitations of armchair [Si(4,4)] $Si_{102}H_{16}$, $Si_{136}H_{16}$, $Si_{168}H_{16}$: (a) along the $E\perp$ tube direction and (b) along the $E||$ tube direction.

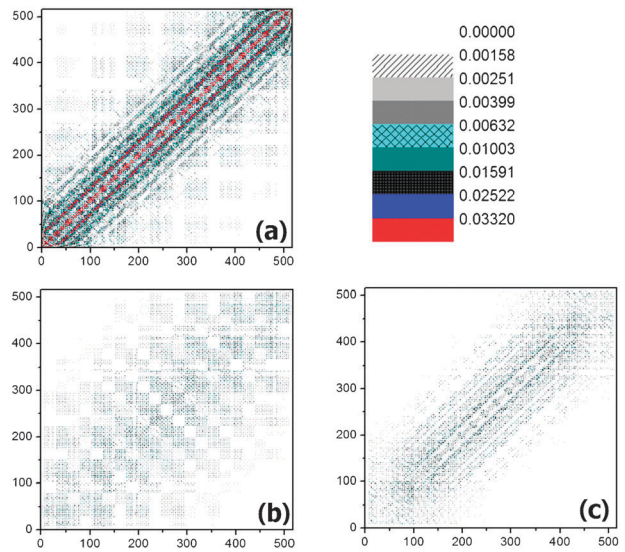

Fig. 9 The ground and induced density matrix ($\Delta\rho$) of armchair $Si_{126}H_{12}$[Si(3,3)] in the parallel tubular axis direction: (a) ground state, (b) 1.001 eV, (c) 2.650 eV (dephasing constant is 0.1 eV in the calculation).

The optical properties of cubic crystal SiNT corresponds to σ–σ* electron transitions of sp^3-hybridized silicons, so the transition energy (2.76 eV) is the highest and the intensity is not strong. Meanwhile, the σ–σ* transition energy (2.06 eV) in sp^2-hybridized SiNTs is lower. The σ–σ* transition energy moves to low energy with a decrease in the SiNW diameter.[48]

Theoretically zigzag SiNTs possess weaker overlap of p_z orbitals and weaker delocalization of π electron, but their electron excitations are similar to those of armchair SiNTs. The optical properties of polycrystalline or amorphous SiNTs will include the peak from π–π* electron transitions of sp^2-hybridized SiNTs, because unsaturated p_z orbitals will overlap somewhat with each other, and form weak delocalized π bonds and result in low-energy π–π* absorption, especially for the large surface-to-size ratio. The peak would probably be observed experimentally in the near-IR region, but the transition intensity of π–π* transition would be stronger than that of σ–σ* transition.

Conclusions

The electron excitations of three kinds of SWSiNTs were calculated using the LDM method and the INDO/S Hamiltonian. The nature of major transitions were characterized by examining their induced single-electron density matrices. It was found that the optical properties of SiNTs are strongly affected by the hybridization type. The main results are summarized as follows:

(1) The electron excitations of SiNTs are sensitive to the hybridization types. The transition intensity in the parallel tubular direction is higher than that in the perpendicular tubular direction for SiNTs based on both sp^2 and sp^3 hybridization. The corresponding major transition peaks red-shift and the intensities increase with an increase in length along the tubular direction.

(2) The optical gaps of the infinitely long pentagonal sp^3-hybridized SWSiNT along the direction of tubular axis are about 3.0 eV and 4.7 eV and originate from σ–σ* electron transitions. The optical gaps of the infinitely long sp^2 armchair [Si(3,3)] SWSiNT along the tubular direction are about 0.7 eV and 2.4 eV, those of [Si(4,4)] are 0.7 eV and 2.7 eV owing to π–π* and σ–σ* electron transitions, separately. The transition intensities of sp^2-hybridized SiNTs are larger than those of sp^3-hybridized SiNTs.

(3) The electron excitations of sp^2-hybridized zigzag SWSiNTs appear to be very similar to those of armchair SWSiNTs, with the main contribution from the overlap of lonely unpaired p_z orbitals. The weak overlap of p_z orbitals has a big effect on electron transition and spectra character in spite of a weaker effect on stability. It reflects that SiNTs based on sp^2 hybridization possess more potential in optical fields than those based on sp^3 hybridization.

Acknowledgements

The authors gratefully acknowledge financial support from the Science and Technology Development Planning of Jilin Province (201201067), the National Natural Science Foundation of China (20903020, 21131001 and 21173035), and 973 Program (2009CB623605).

References

1 S. Iijima, *Nature*, 1991, **354**, 56–58.
2 D. Tasis, N. Tagmatarchis, A. Bianco and M. Prato, *Chem. Rev.*, 2006, **106**, 1105–1136.
3 J. Goldberger, R. Fan and P. D. Yang, *Acc. Chem. Res.*, 2006, **39**, 239–248.
4 I. Kiricsi, A. Fudala, D. Mehn, A. Kukovecz, Z. Konya, M. Hodos, E. Horvath, M. Urban, T. Kanyo, E. Molnar and R. Smajda, *Curr. Appl. Phys.*, 2006, **6**, 212–215.
5 M. Zhang, Z. M. Su, L. K. Yan, Y. Q. Qiu, G. H. Chen and R. S. Wang, *Chem. Phys. Lett.*, 2005, **408**, 145–149.
6 R. Tenne, M. Remskar, A. Enyashin and G. Seifert, in *Carbon Nanotubes*, ed. A. D. G. D. M. S. Jorio, 2008, vol. 111, pp. 631–671.
7 D. F. Perepichka and F. Rosei, *Small*, 2006, **2**, 22–25.
8 M. Ni, G. Luo, J. Lu, L. Lai, L. Wang, M. Jing, W. Song, Z. Gao, G. Li, W. N. Mei and D. Yu, *Nanotechnology*, 2007, **18**, 505707.
9 M. Xie, J. Wang, Z. Fan, J. G. Lu and Y. K. Yap, *Nanotechnology*, 2008, **19**, 365609.
10 V. Verma, K. Dharamvir and V. K. Jindal, *J. Nano Res.*, 2008, **2**, 85–90.
11 G. P. Lithoxoos, J. Samios and Y. Carissan, *J. Phys. Chem. C*, 2008, **112**, 16725–16728.
12 Y. Li, Z. Zhou, Y. Chen and Z. Chen, *J. Chem. Phys.*, 2009, **130**, 204706.
13 R. K. F. Lee, B. J. Cox and J. M. Hill, *J. Phys.: Condens. Matter*, 2009, **21**, 075301.

14 S. Cahangirov, M. Topsakal, E. Akturk, H. Sahin and S. Ciraci, *Phys. Rev. Lett.*, 2009, **102**, 236804.
15 R. West and M. J. Fink, *Science*, 1981, **214**, 1343–1344.
16 C. H. Lai, M. D. Su and S. Y. Chu, *Organometallics*, 2002, **21**, 397–400.
17 M. Ichinohe, R. Kinjo and A. Sekiguchi, *Organometallics*, 2003, **22**, 4621–4623.
18 S. Tsutsui, E. Kwon, H. Tanaka, S. Matsumoto and K. Sakamoto, *Organometallics*, 2005, **24**, 4629–4638.
19 H. Ottosson and P. G. Steel, *Chem.–Eur. J.*, 2006, **12**, 1576–1585.
20 S. B. Fagan, R. J. Baierle, R. Mota, A. J. R. da Silva and A. Fazzio, *Phys. Rev. B: Condens. Matter*, 2000, **61**, 9994–9996.
21 S. B. Fagan, R. Mota, R. J. Baierle, G. Paiva, A. J. R. da Silva and A. Fazzio, *THEOCHEM*, 2001, **539**, 101–106.
22 G. Seifert, T. Kohler, H. M. Urbassek, E. Hernandez and T. Frauenheim, *Phys. Rev. B: Condens. Matter*, 2001, **63**, 193409.
23 J. W. Kang, J. J. Seo and H. J. Hwang, *J. Nanosci. Nanotechnol.*, 2002, **2**, 687–691.
24 R. Q. Zhang, S. T. Lee, C. K. Law, W. K. Li and B. K. Teo, *Chem. Phys. Lett.*, 2002, **364**, 251–258.
25 A. S. Barnard and S. P. Russo, *J. Phys. Chem. B*, 2003, **107**, 7577–7581.
26 K. R. Byun, J. W. Kang and H. J. Hwang, *J. Korean Phys. Soc.*, 2003, **42**, 635–646.
27 J. W. Kang and H. J. Hwang, *Nanotechnology*, 2003, **14**, 402–408.
28 M. Zhang, Y. H. Kan, O. J. Zang, Z. M. Su and R. S. Wang, *Chem. Phys. Lett.*, 2003, **379**, 81–86.
29 J. W. Kang, K. R. Byun and H. J. Hwang, *Modell. Simul. Mater. Sci. Eng.*, 2004, **12**, 1–12.
30 Y. R. Jeng, P. C. Tsai and T. H. Fang, *Phys. Rev. B: Condens. Matter Mater. Phys.*, 2005, **71**, 085411.
31 X. B. Yang and J. Ni, *Phys. Rev. B: Condens. Matter Mater. Phys.*, 2005, **72**, 195426.
32 R. Q. Zhang, H. L. Lee, W. K. Li and B. K. Teo, *J. Phys. Chem. B*, 2005, **109**, 8605–8612.
33 P. Pradhan and A. K. Ray, *J. Comput. Theor. Nanosci.*, 2006, **3**, 128–133.
34 A. Palaria, G. Klimeck and A. Strachan, *Phys. Rev. B: Condens. Matter Mater. Phys.*, 2008, **78**, 205315.
35 C.-H. Zhang and J. Shen, *Chem. Phys. Lett.*, 2009, **478**, 61–65.
36 E. Durgun, S. Tongay and S. Ciraci, *Phys. Rev. B: Condens. Matter Mater. Phys.*, 2005, **72**, 075420.
37 G. Seifert, T. Frauenheim, T. Kohler and H. M. Urbassek, *Phys. Status Solidi B*, 2001, **225**, 393–399.
38 O. Ponomarenko, M. W. Radny and P. V. Smith, *Surf. Sci.*, 2004, **562**, 257–268.
39 J. Bai, X. C. Zeng, H. Tanaka and J. Y. Zeng, *Proc. Natl. Acad. Sci. U. S. A.*, 2004, **101**, 2664–2668.
40 M. Menon, A. N. Andriotis and G. Froudakis, *Nano Lett.*, 2002, **2**, 301–304.
41 A. N. Andriotis, G. Mpourmpakis, G. E. Froudakis and M. Menon, *New J. Phys.*, 2002, **4**, 78.1–78.14.
42 A. K. Singh, T. M. Briere, V. Kumar and Y. Kawazoe, *Phys. Rev. Lett.*, 2003, **91**, 146802.
43 G. Mpourmpakis, G. E. Froudakis, A. N. Andriotis and M. Menon, *J. Chem. Phys.*, 2003, **119**, 7498–7502.
44 A. K. Singh, V. Kumar and Y. Kawazoe, *J. Mater. Chem.*, 2004, **14**, 555–563.
45 J. Bai and X. C. Zeng, *Nano*, 2007, **2**, 109–114.
46 J. Sha, J. J. Niu, X. Y. Ma, J. Xu, X. B. Zhang, Q. Yang and D. Yang, *Adv. Mater.*, 2002, **14**, 1219–1221.
47 S. Y. Jeong, J. Y. Kim, H. D. Yang, B. N. Yoon, S. H. Choi, H. K. Kang, C. W. Yang and Y. H. Lee, *Adv. Mater.*, 2003, **15**, 1172–1176.
48 B. K. Teo, C. P. Li, X. H. Sun, N. B. Wong and S. T. Lee, *Inorg. Chem.*, 2003, **42**, 6723–6728.
49 J. Q. Hu, Y. Bando, Z. W. Liu, J. H. Zhan, D. Golberg and T. Sekiguchi, *Angew. Chem., Int. Ed.*, 2004, **43**, 63–66.
50 Y. W. Chen, Y. H. Tang, L. Z. Pei and C. Guo, *Adv. Mater.*, 2005, **17**, 564–567.
51 Y. H. Tang, L. Z. Pei, Y. W. Chen and C. Guo, *Phys. Rev. Lett.*, 2005, **95**, 116102.
52 M. De Crescenzi, P. Castrucci, M. Scarselli, M. Diociaiuti, P. S. Chaudhari, C. Balasubramanian, T. M. Bhave and S. V. Bhoraskar, *Appl. Phys. Lett.*, 2005, **86**, 231901.
53 C. Mu, Y. X. Yu, W. Liao, X. S. Zhao, D. S. Xu, X. H. Chen and D. P. Yu, *Appl. Phys. Lett.*, 2005, **87**, 113104.
54 T. Qiu, X. L. Wu, Y. F. Mei, G. J. Wan, P. K. Chu and G. G. Siu, *J. Cryst. Growth*, 2005, **277**, 143–148.
55 C. Li, Z. T. Liu, C. Gu, X. Xu and Y. Yang, *Adv. Mater.*, 2006, **18**, 228–234.
56 P. Castrucci, M. Scarselli, M. De Crescenzi, M. Diociaiuti, P. S. Chaudhari, C. Balasubramanian, T. M. Bhave and S. V. Bhoraskar, *Thin Solid Films*, 2006, **508**, 226–230.
57 S. Yamada and H. Fujiki, *Jpn. J. Appl. Phys.*, 2006, **45**, L837–L839.
58 M. Ben Ishai and F. Patolsky, *J. Am. Chem. Soc.*, 2009, **131**, 3679–3689.
59 Y. W. Tang, Z. Huang, X. W. Wang and X. C. Zeng, *J. Comput. Theor. Nanosci.*, 2006, **3**, 824–829.
60 N. Wang, Y. Cai and R. Q. Zhang, *Mater. Sci. Eng., R*, 2008, **60**, 1–51.
61 S. Mukamel, *Principle of Nonlinear Optical Spectroscopy*, Oxford University Press, New York, 1995.
62 S. H. Lin, R. Alden, R. Islampour, H. Ma and A. A. Villaeys, *Matrix Method and Femtosecond Processes*, World Scientific, Singapore, 1991.
63 P. Ring and P. Schuck, *The Nuclear Many-Body Problem*, Springer, New York, 1980.
64 J. A. Pople and G. A. Segal, *J. Chem. Phys.*, 1965, **43**, S136–S151.
65 J. A. Pople, D. L. Beveridg and P. A. Dobosh, *J. Chem. Phys.*, 1967, **47**, 2026–2033.
66 J. Ridley and M. Zerner, *Theor. Chim. Acta*, 1973, **32**, 111–134.
67 W. Z. Liang, S. Yokojima, D. H. Zhou and G. H. Chen, *J. Phys. Chem. A*, 2000, **104**, 2445–2453.
68 S. Yokojima and G. H. Chen, *Phys. Rev. B: Condens. Matter*, 1999, **59**, 7259–7262.
69 S. Yokojima and G. H. Chen, *Chem. Phys. Lett.*, 1998, **292**, 379–383.
70 M. F. Ng, Y. Zhao and G. H. Chen, *J. Phys. Chem. B*, 2003, **107**, 9589–9600.
71 A. D. Bacon and M. C. Zerner, *Theor. Chim. Acta*, 1979, **53**, 21–54.
72 M. J. Frisch, G. W. Trucks, H. B. Schlegel, G. E. Scuseria, M. A. Robb, J. R. Cheeseman, J. Montgomery, J. A. T. Vreven, K. N. Kudin, J. C. Burant, J. M. Millam, S. S. Iyengar, J. Tomasi, V. Barone, B. Mennucci, M. Cossi, G. Scalmani, N. Rega, G. A. Petersson, H. Nakatsuji, M. Hada, M. Ehara, K. Toyota, R. Fukuda, J. Hasegawa, M. Ishida, T. Nakajima, Y. Honda, O. Kitao, H. Nakai, M. Klene, X. Li, J. E. Knox, H. P. Hratchian, J. B. Cross, V. Bakken, C. Adamo, J. Jaramillo, R. Gomperts, R. E. Stratmann, O. Yazyev, A. J. Austin, R. Cammi, C. Pomelli, J. W. Ochterski, P. Y. Ayala, K. Morokuma, G. A. Voth, P. Salvador, J. J. Dannenberg, V. G. Zakrzewski, S. Dapprich, A. D. Daniels, M. C. Strain, O. Farkas, D. K. Malick, A. D. Rabuck, K. Raghavachari, J. B. Foresman, J. V. Ortiz, Q. Cui, A. G. Baboul, S. Clifford, J. Cioslowski, B. B. Stefanov, G. Liu, A. Liashenko, P. Piskorz, I. Komaromi, R. L. Martin, D. J. Fox, T. Keith, M. A. Al-Laham, C. Y. Peng, A. Nanayakkara, M. Challacombe, P. M. W. Gill, B. Johnson, W. Chen, M. W. Wong, C. Gonzalez and J. A. Pople, *Gaussian 03*, Gaussian, Inc., Wallingford CT, 2004.
73 M. F. Ng and R. Q. Zhang, *J. Phys. Chem. B*, 2006, **110**, 21528–21535.
74 K. Uchiyama, S. Nagendran, S. Ishida, T. Iwamoto and M. Kira, *J. Am. Chem. Soc.*, 2007, **129**, 10638–10639.
75 C. Delerue, G. Allan and M. Lannoo, *Phys. Rev. B: Condens. Matter*, 1993, **48**, 11024–11036.
76 R. M. Minyaev, V. I. Minkin, T. N. Gribanova, A. G. Starikov and R. Hoffmann, *J. Org. Chem.*, 2003, **68**, 8588–8594.
77 H. Gilman, W. H. Atwell and G. L. Schwebke, *J. Organomet. Chem.*, 1964, **2**, 369–371.
78 C. C. Phifer, W. J. Thomes, K. Simmons-Potter and B. G. Potter, *J. Chem. Phys.*, 2004, **120**, 1613–1616.
79 J. D. Holmes, K. P. Johnston, R. C. Doty and B. A. Korgel, *Science*, 2000, **287**, 1471–1473.
80 W. Z. Liang, S. Yokojima, M. F. Ng, G. H. Chen and G. Z. He, *J. Am. Chem. Soc.*, 2001, **123**, 9830–9836.

